The Respective Roles of CYP3A4 and CYP2D6 in the Metabolism of Pimozide to Established and Novel Metabolites

Drug Metabolism and Disposition

Brian D. Chapron, Jean C. Dinh, Paul C. Toren, Andrea Gaedigk and J. Steven Leeder

Supplementary Information

Supplemental Tables

Supplemental Table 1. Cone Voltage and Collision Energy for Analysis of Analyte Fragmentation on XEVO-TQD

Parameter	DHPBI	Hydroxypimozide	Pimozide
Parent (*m/z*)	218.1	478.3	462.3
Cone Voltage (V)	40	70	70
Capillary Voltage (kV)	2.41	2.41	2.41
Collision Energy (V)	15	30	30
Mode	ESI+	ESI+	ESI+
RF (V)	2.5	2.5	2.5
Extractor (V)	3	3	3
Source Temperature (°C)	150	150	150
Desolvation Temperature (°C)	400	400	400
Cone Gas Flow (L/h)	0	0	0
Desolvation Gas Flow (L/h)	800	800	800

Supplemental Table 2. Cone Voltage and Collision Energy for Analyte Quantification on XEVO-TQ-XS

Parameter	DHPBI	DHPBI-d_5	Hydroxypimozide	Pimozide	Pimozide-d_5
Parent (*m/z*)	218.1	223.1	478.3	462.3	469.3
Product ion (*m/z*)	84	89	328.1	328.1	333.1
Retention Time (min)	1.61	1.61	5-OH: 4.71 6-OH: 4.83	6.7	6.7
Cone Voltage (V)	45	45	70	70	70
Capillary Voltage (kV)	1.25	1.25	1.25	1.25	1.25
Collision Energy (V)	18	18	30	30	30
Mode	ESI+	ESI+	ESI+	ESI+	ESI+
Source Offset (V)	30	30	30	30	30
Source Temperature (°C)	150	150	150	150	150
Desolvation Temperature (°C)	500	500	500	500	500
Cone Gas Flow (L/h)	150	150	150	150	150
Desolvation Gas Flow (L/h)	1000	1000	1000	1000	1000

Supplemental Figures

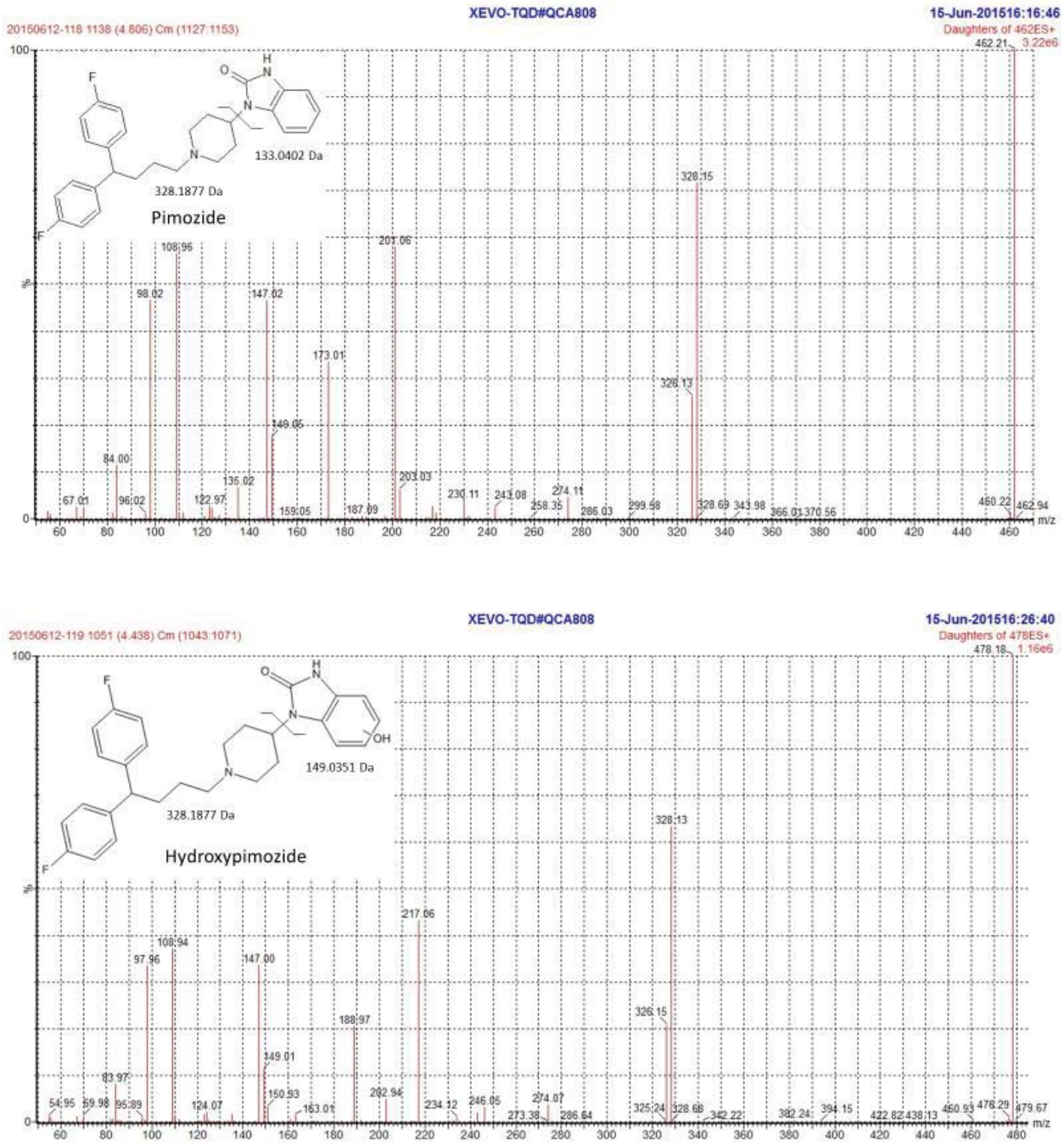

Supplemental Figure 1. Daughter ions produced from pimozide (top) and the hydroxypimozide (bottom) metabolite(s) suggest the benzimidazolone ring is a site of ring hydroxylation in human liver microsomes isolated from a donor genotyped as a *CYP2D6* ultra rapid metabolizer (UM) and incubated with 10 μM pimozide.

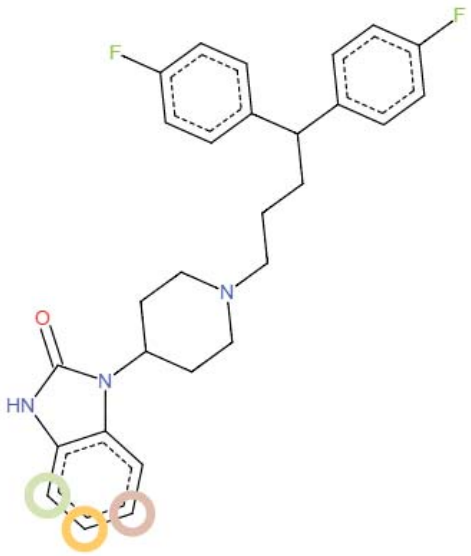

Standard CYP2C CYP2D6

1: null

Rank	Atom	Score	Energy	S2End	N+Dist	2DSASA
1	**C.27**	**84.96**	**86.3**	**0**	**8**	**33.5**
2	**C.26**	**86.19**	**74.1**	**1**	**7**	**32.67**
3	**C.28**	**98.59**	**86.3**	**1**	**7**	**27.83**
4	C.3	102.96	84.1	2	7	31.1
5	C.25	112.1	86.3	2	6	25.09
6	C.8	113.34	59.9	5	4	5.18
7	C.20	113.7	41.1	7	1	29.29
8	C.18	113.95	41.1	8	1	23.33
9	N.30	115.59	89.6	2	6	20.21
10	C.4	118.81	86.3	3	6	24.72
11	C.16	135.61	75.9	6	3	16.2
12	C.22	135.92	75.9	5	3	8.19
13	C.21	141.97	75.9	6	2	24.63
14	C.17	142.2	75.9	7	2	19.3
15	N.23	143.23	89.6	4	4	0.25
16	N.19	230.62	150.3	8	0	3.92
17	C.2	1,005.36	999	1	8	8.48
18	C.29	1,025.54	999	2	6	6.44
19	C.31	1,038.87	999	3	5	8.2
20	C.24	1,039	999	3	5	5.09
21	C.5	1,045.84	999	4	5	2.48

Supplemental Figure 2. SmartCYP predictions for sites of metabolism by CYP2D6. Likelihood of being the principle site of site of oxidation decreases with increasing rank number. The top three most likely sites for oxidation are color-coded as follows: 4-hydroxylation (green), 5-hydroxylation (yellow) and 6-hydroxylation (reddish-brown) and denoted with circles on the pimozide molecule on the left-hand side.

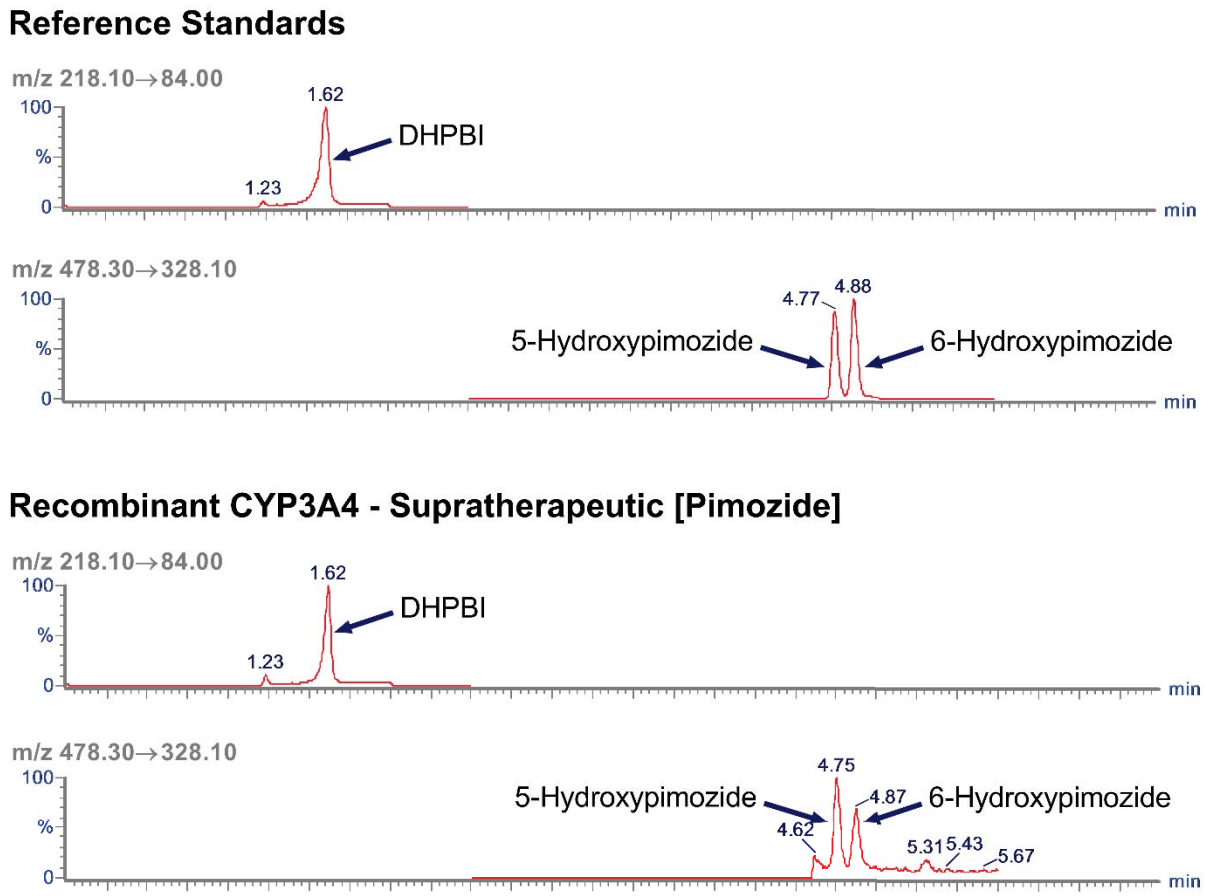

Supplemental Figure 3. Elution of hydroxypimozide isomers and DHPBI with products of CYP3A4-mediated metabolism at supratherapeutic concentrations of pimozide. Chromatograms for combined standards of 50 nM DHPBI (*m/z* 218.10 → 84.00) and 5-/6-hydroxypimozide metabolites (*m/z* 478.30 → 328.10) are shown (upper panel) for reference. Incubations of 100 nM pimozide 2 pmol/mL recombinant CYP3A4 (bottom panel) are displayed beneath. Retention times are listed in blue above the respective peaks.

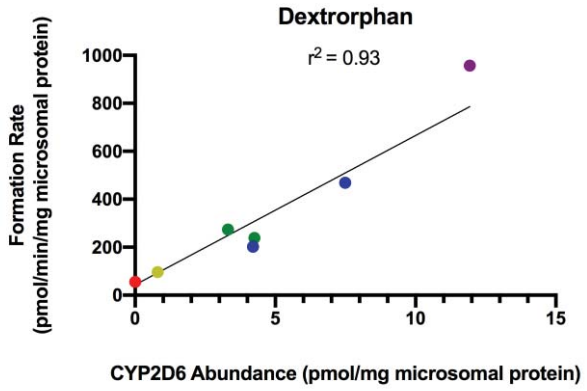

Supplemental Figure 4. Correlation of CYP2D6 protein abundance and the rate of dextromethorphan *O*-demethylation to dextrorphan in HLMs isolated from individual donors (n = 7). Dextrorphan formation rates reflect a single vendor-supplied value. The r^2 corresponding to the fit of a linear regression model is listed at the top of the graph. Expression of CYP2D6 protein was determined via MS/MS analysis. Data points were color coded to reflect activity score assignments for *CYP2D6* genotypes: 0 (red), 0.5 (yellow), 1.0 (green), 2.0 (blue) and >2.25 (purple) (Caudle et al., 2020).

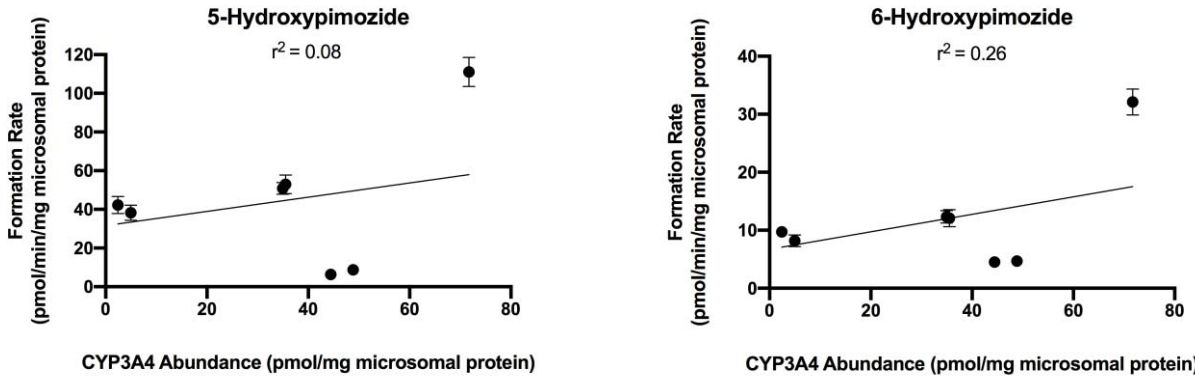

Supplemental Figure 5. Correlation of CYP3A4 protein abundance and the rate of pimozide 5-hydroxylation (left) and 6-hydroxylation (right) in HLMs isolated from individual donors (n = 7). Data points represent the mean of separate experiments (n = 3) and error bars reflect the SD; error bars are not visible for many points due to low inter-experimental variability. The r^2 corresponding to the fit of a linear regression model for each metabolite is listed at the top of each respective graph. Expression of CYP3A4 protein was determined via MS/MS analysis.

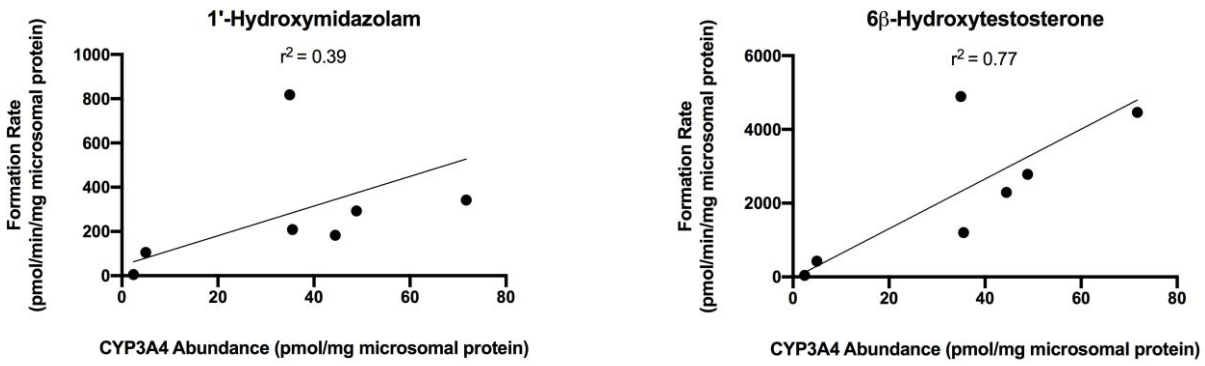

Supplemental Figure 6. Correlation of CYP3A4 protein abundance and the rate of midazolam 1'-hydroxylation (left) and testosterone 6β-hydroxylation (right) in HLMs isolated from individual donors (n = 7). The rates of 1'-hydroxymidazolam and 6β-hydroxytestosterone represent singular vendor-supplied values. Expression of CYP3A4 protein was determined via MS/MS analysis.

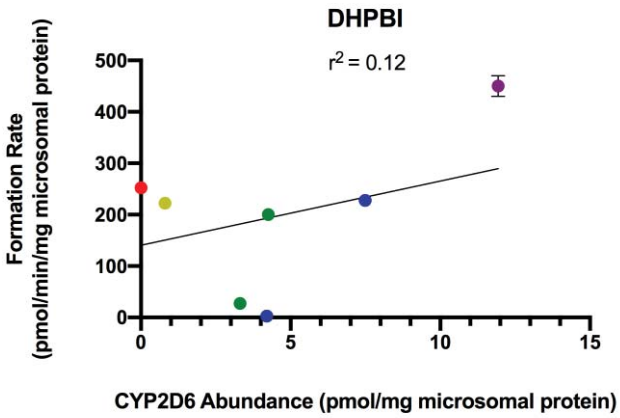

Supplemental Figure 7. Correlation of CYP2D6 protein abundance and the rate of DHPBI formation in HLMs isolated from individual donors (n = 7). Data points represent the mean of separate experiments (n = 3) and error bars reflect the SD; error bars are not visible for many points due to low inter-experimental variability. The r^2 corresponding to the fit of a linear regression model is listed at the top of the graph. Expression of CYP2D6 protein was determined via MS/MS analysis. Data points were color coded to reflect activity score assignments for CYP2D6 genotypes: 0 (red), 0.5 (yellow), 1.0 (green), 2.0 (blue) and >2.25 (purple) (Caudle et al., 2020).

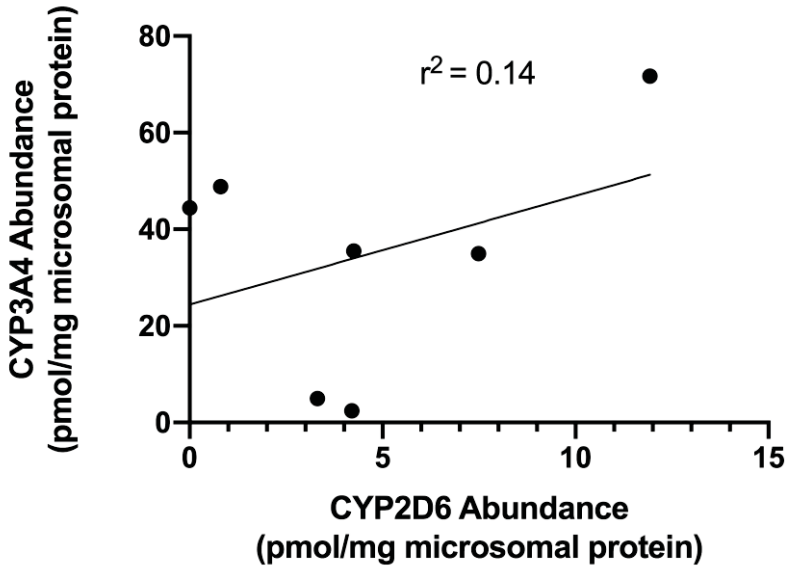

Supplemental Figure 8. Correlation of CYP3A4 and CYP2D6 protein abundance. Abundances of CYP2D6 and CYP3A4 proteins were determined via MS/MS analysis.